Statistical analysis of the strength and lifetime under tension of crystalline polymeric solids

C Y Li[1,2] and K H Nitta[1]

[1]Institute of Science and Engineering, Kanazawa University, Kakuma Campus, Kanazawa, 920-1192, JP

[1]E-mail: nitta@se.kanazawa-u.ac.jp

Abstract. The ductile fracture behavior under uniaxial tension of melt-crystallized isotactic polypropylene specimens at room temperature was investigated from a statistical point of view. Each tensile test was performed more than one hundred times and statistical data for the breaking point were obtained under each tensile condition. The probability distribution curves of the fracture time and strength approximately followed Gaussian statistics at lower tensile speeds, but changed to a Weibull function at higher-speed tests. Additionally, with increasing tensile speed the mean and standard deviation of the fracture time decreased linearly. The toughness, which is the total area under the stress-strain curves, was found to be independent of the tensile conditions, indicating that fracture toughness is a criterion for fracture under tension.

1. Introduction

Characterization of tensile fracture behavior in commodity semicrystalline plastics is important for their extension to engineering and industrial applications. Semicrystalline polymers show high ductility with yielding, necking and strain hardening under typical tensile conditions. In accordance with the amount of plastic deformation involved in various tensile conditions, fracture characteristics can be broadly categorized as brittle or ductile. The two categories can be distinguished by whether or not yielding and necking is involved. However, the fracture behavior of semicrystalline polymers cannot easily be classified as either ductile or brittle. Nitta et al [1] found that high density PE materials can be broken in a brittle fashion at higher strain rates and lower temperatures but show a clear yield peak. In this case, they are called semi-brittle.

Over the past decades, statistical analyses of fracture processes in plastics, rubbers, metals, ceramics, fibers and composites have received attention because the statistical data play a critical role in designing materials with high reliability and long life time for engineering applications [2]. The characteristics and corresponding structural models for brittle or quasi-brittle fractures have been comprehensively and extensively studied; in particular by Bazant [3] and Pheonix [4]. Bazant et al. [3,5] suggested that the specimen size of brittle and/or quasi-brittle materials strongly affects the

[1] To whom any correspondence should be addressed.

[2] Present address: Toray Battery Separator Film Co., Ltd. Nasu-Shiobara, Tochigi, 329-2763, JP

strength distribution function. Their work focused on probabilistic formulations for practical assessments of uncertainties in strength predictions using the classical weakest link theory [6]. The behavior of brittle fracture was analyzed using Weibull distribution functions [7]. However, few statistical studies have been performed on the ductile fracture behavior of commodity plastics in typical tensile tests [8].

In this work, isotactic polypropylene (iPP) was chosen as a model plastic material. The ability to predict the fracture points of such iPP materials under uniaxial extension is of critical importance to determine reliability and efficiency for practical use. Therefore, it is useful to find the characteristics of fracture behavior of iPP that relate directly to the service performance of the material. Mechanical experiments such as the uniaxial elongation test are useful to determine optimal conditions for drawing of the plastics. In this work, we examined the probability functions for tensile breakage data such as fracture time, strength, and toughness of iPP films under various tensile conditions.

2. Experimental

Commercial grade iPP with $M_w=4.0\times10^5$ and $M_w/M_n=5$ was used in this work. The iPP films were prepared by compression molding at 230°C for 5 min, and quenching in boiling water (100°C). The film thickness was controlled to be about 200 μm. The crystallinity of the films was 59% (estimated from density) and their melting temperature was 162°C (estimated from differential scanning calorimetry). Double-edge notched specimens were cut from films for the tensile measurements. We employed a double-edge notched specimen with gauge length L_0 = 4 mm, 4-mm width and 200-μm thickness. The uniaxial elongation tests for these specimens were repeated more than 100 times at room temperature under each test condition. The tensile speed was varied from 15 mm/min to 70 mm/min. Additionally, tensile tests were performed at higher tensile speeds of 140 and 170 mm/min. The time to fracture was read out from the tensile load-time data. The tensile strength was determined by dividing the tensile load at the breaking point by the initial cross-sectional area.

The data from the tensile tests were analyzed statistically by taking the class size to be 10, corresponding to the square of the sample size. Distribution analysis of the fracture data was carried out using OriginPro 8 commercial software (OriginLab Co. Ltd, USA).

3. Results and discussion

3.1 Probability distribution functions of fracture time and strength

All stress-elongation time curves were measured more than 100 times with fixed crosshead speed. The ten stress-time curves measured at 15-mm min^{-1} crosshead speed are shown in figure 1. The iPP specimens showed a distinct yield point as a maximum in the stress-strain curves beyond the elastic limit. When using notched specimens, the neck constitutes the entire portion of the gauge length immediately after the neck is initiated [1]. Thus, the necked region in the stress-strain curves can be neglected. Therefore, the yield region after the initial elastic region is followed by a virtually complete strain-hardening deformation, and as a result the stress linearly increases as elongation proceeds after the yield process. As seen in this figure, the fracture time has a wide scatter, and thus the probability distribution data for the fracture time as well as the fracture stress (strength) were fit to a typical Gaussian distribution (figure 2).

The shape of the curve of the tensile stress versus elongation time (figure 1) is roughly composed of a yield peak, hardening region, and a negligible necking region. Therefore, we found a linear relationship between stress and elongation time in the hardening region near the breaking point:

$$\sigma = G_p t + \omega_p , \tag{1}$$

where G_p is the slope of the stress-time curve in the hardening region and ω_p is the intercept on the stress axis. The fluctuation of G_p is very small compared with the time to fracture, t_B, and ω_p, with G_p =

0.128 ± 0.01 MPa s^{-1}.

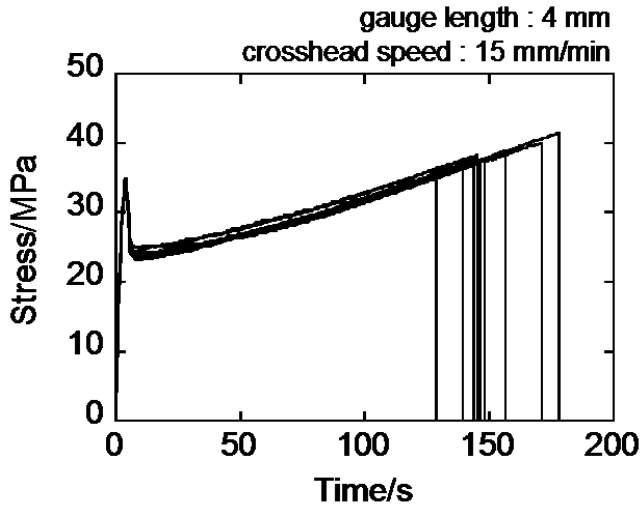

Figure 1. Stress-strain curves for iPP specimens with 4-mm gauge length, measured at 15-mm/min crosshead speed at room temperature .

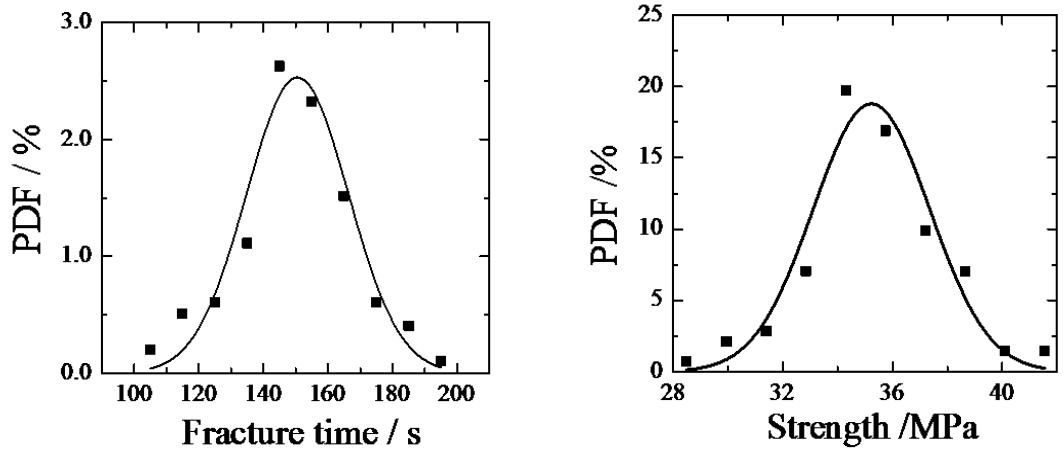

Figure 2. Probability density functions of fracture time and fracture strength for 15-mm/min crosshead speed. The solid line is the fit to a Gaussian distribution function.

Consequently, the tensile strength is linearly transferred over the time to fracture, t_B, offset by the ω_p values. When we consider the fluctuation of ω_p as a noise fluctuation, this process can be treated as a well-known Kalman filter problem [9]. Because the noise in ω_p is a result of fluctuation of the load cell and specimen thickness, ω_p is independent of t_B. Furthermore, the fact that the probability density function of the fracture strength can be fit by a Gaussian distribution implies that ω_p is Gaussian. If the relation between the stress and elongation time closely followed a concave or convex curve, the

distribution would have negative or positive skewness, respectively, leading to a derivative Weibull fit [10].

3.2 Tensile speed dependence

With increasing tensile speed, fracture time decreased and the dispersion in the PDF curves narrowed. Furthermore, the mean fracture time $\bar{t}_B$ and its standard deviation Δ_t are proportional to the inverse of the tensile speed *v*, given by $v\bar{t}_B = \lambda_0$ where λ_0 = 37 mm, and $\Delta_t = \delta_0 / v$ where δ_0 =3.2 mm (see figure 3). Consequently, the PDF curves of the fracture time can be written in terms of the reciprocal quantity $\tau = 1/v$ as

$$p_t(t_B;\tau) = \frac{1}{\sqrt{2\pi(\delta_0\tau)^2}} \exp\left[-\frac{(t_B - \lambda_0\tau)^2}{2(\delta_0\tau)^2} \right]. \tag{2}$$

Here τ is the intrinsic time. In the tensile tests, the elongation velocity *v* is above zero so that the intrinsic time τ has a time horizon. Hence, as $v \to \infty$, the limit of the intrinsic time is given by τ = 0. Here we can assume the initial condition t_B = 0 when τ = 0, according to the straight line to the origin. The PDF satisfies the partial differential equation

$$\frac{\partial}{\partial\tau} p_t(t_B;\tau) = \left\{ -\lambda_0 \frac{\partial}{\partial t_F} + \delta_0^2 \tau \frac{\partial^2}{\partial {t_F}^2} \right\} p_t(t_B;\tau). \tag{3}$$

This is a *Kolmogorov forward equation* [11], in which the fracture behavior in the ductile experiment can be regarded as a diffusion process in which fracture events correspond to particle diffusion, intrinsic time τ(=1/*v*) corresponds to the diffusion time, and the fracture time t_B corresponds to the diffusion distance.

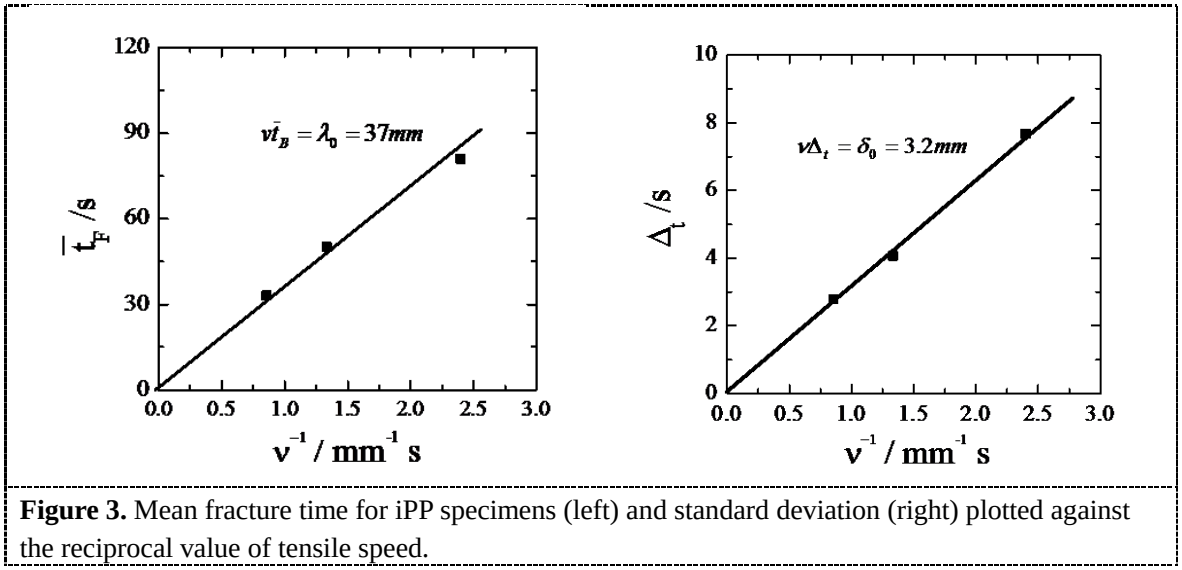

Figure 3. Mean fracture time for iPP specimens (left) and standard deviation (right) plotted against the reciprocal value of tensile speed.

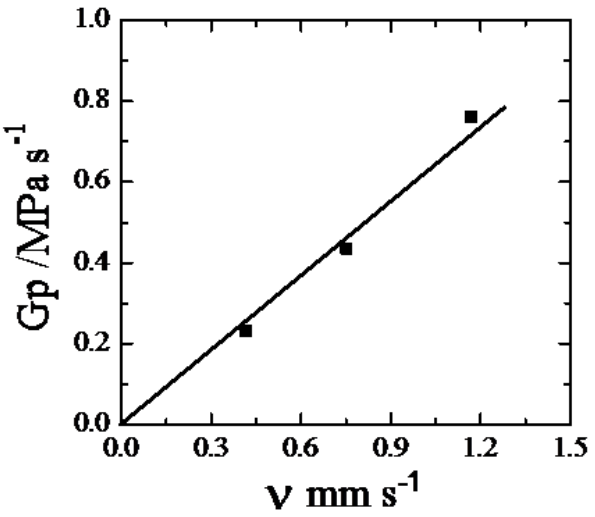

Figure 4. Strain-hardening slope Gp of iPP specimens plotted against tensile speed *v*.

Figure 4 shows the dependence of the strain-hardening slope G_p on tensile speed. We found a linear proportionality between G_p and v with the empirical relation $G_p = \gamma_0 v$, where γ_0 = 670 MPa/m. As a result, equation (1) can be rewritten as

$$\sigma = \gamma_0 vt + \omega_p = \gamma_0 L_0 \frac{vt}{L_0} + \omega_p = \gamma_0 L_0 \varepsilon + \omega_p , \tag{4}$$

where L_0 is the initial gauge length. Because the product of v and t is the increment of the gauge length under tension, the strain ε can be given by vt/L_0, and thus the stress value is proportional to the strain ε, and Haward's stress-hardening modulus [12] corresponds to $\gamma_0 L_0 / 3$. The stochastic behavior of stress is obtained from the stochastic fracture time plus the Gaussian noise ω_p via the linear relation of equation (1), revealing the mean and variance of strength:

$$\bar{\sigma}_B = \mathrm{E}\left[G_p t_B + \omega_p\right] = \gamma_0 \varepsilon_0 L_0 + \bar{\omega}_p , \tag{5}$$

$$\Delta_\sigma^2 = \mathrm{E}\left[\left(\sigma_F - \bar{\sigma}_F\right)^2\right] = \gamma_0^2 \delta_0^2 + \Delta_\omega^2 . \tag{6}$$

Considering that the noise fluctuation ω_p can be caused by experimental errors such as fluctuations of the load cell and specimen thickness, $\bar{\omega}_p$ and Δ_ω^2 are likely to be independent of L_0. Hence, the mean of the strength is predicted to be proportional to the gauge length and its variance is independent of the gauge length.

The concept of toughness is defined in several ways, one of which is the tensile toughness defined as

$$U_F = \int_0^{\varepsilon_F} \sigma(\varepsilon) d\varepsilon . \tag{7}$$

The tensile toughness, which is the energy per volume required to break a specimen, is a measure of the ability of a material or fabricated article to withstand load application in the form of tensile resistance. Interestingly, not only the mean value but also the standard deviation of the fracture toughness were almost independent of the tensile speed as shown in figure 5. This independence implies that fracture toughness is an intrinsic characteristic and a criterion for fracture under the present tensile conditions.

As shown in figure 3, the mean fracture time and its standard deviation were proportional to the reciprocal tensile speed. The fracture events at various speeds were determined by the fracture toughness, and the toughness values were constant, independent of the tensile speed. So as speed is increased, the fracture time required to reach the criteria of toughness will be shorter. Therefore, the mean fracture time is proportional to the reciprocal of the tensile speed. The stretched sample consists of a number of oriented cavities (see figures 9 and 10). As the tensile speed is increased, the time period between fracture events shortens, therefore the fracture time standard deviation becomes narrower with higher tensile speed.

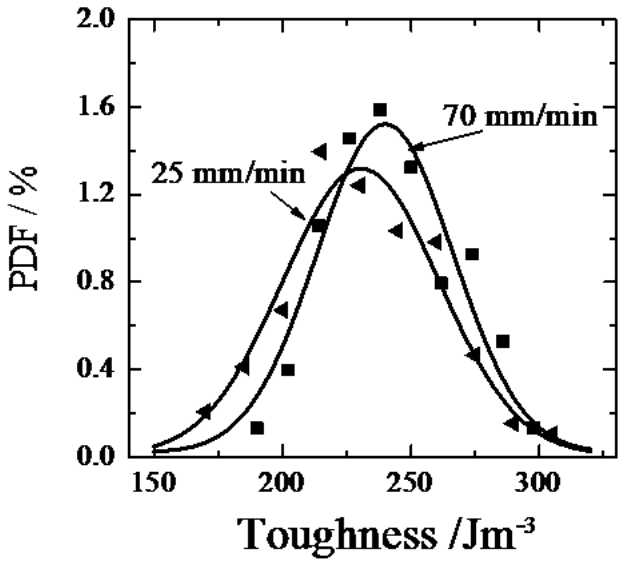

Figure 5. Dependence of toughness distribution of iPP specimens on tensile speed, at tensile speeds of 25 and 70 mm/min.

3.3 Higher tensile speed

Figure 6 compares the PDF curves of fracture time measured at higher tensile speeds of 140 and 170 mm/min. The fracture time data at a crosshead speed of 140 mm/min were symmetric and fit to a typical Gaussian distribution with a skewness value around zero, similar to the fracture time data measured at tensile speeds ranging from 15 to 70 mm/min. The symmetric fracture time scatter for the 170-mm/min data leans to the left with a skewness value of 1.39, and the solid curve is the nest normalized Weibull function given by

$$p_t(t_B) = \frac{m}{\eta}\left(\frac{t_B}{\eta}\right)^{m-1} \exp\left\{-\left(\frac{t_B}{\eta}\right)^{m}\right\}, \tag{8}$$

where *m* is the shape parameter and η is the scale parameter of the distribution. The transition of the PDF curve from a Gaussian to a Weibull function occurred at a tensile speed between 140 and 170 mm/min. This transition seems to be associated with the transition from ductile to semi-brittle [13]. Also, the mean values of the fracture time at higher tensile speeds fall on the same line $\bar{t}_B = \lambda_0 / v$ plotted by the inverse of the tensile speed v^{-1}, with the empirical relationship obtained at the tensile speed range from 15 to 70 mm/min.

The standard deviation of fracture toughness data measured at speeds of 170 and 140 mm/min are 43 and 51 Jm^{-3}, respectively; larger than all the values of toughness measured at lower speeds (about 25 Jm^{-3}). However, there is no clear difference in the mean values of the fracture toughness for the specimens stretched at lower and higher tensile speeds.

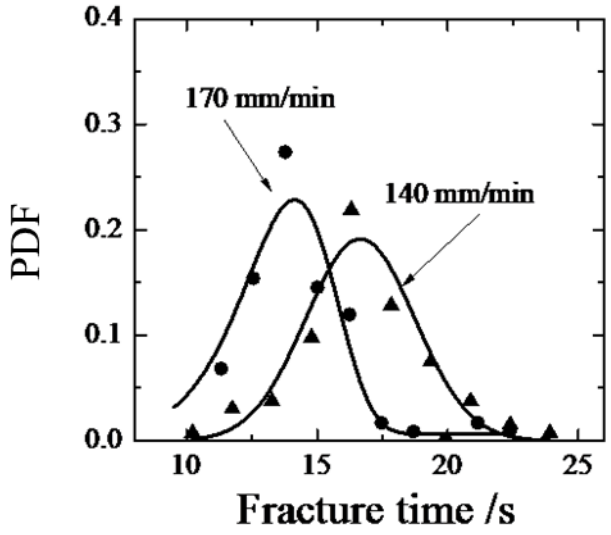

Figure 6. PDF curves of the time distribution of iPP specimens, showing dependence on tensile speed. PDF curve at 140-mm/min tensile speed was fit to a Gaussian distribution and PDF at 170-mm/min tensile speed was fit by a Weibull distribution with m = 8.605 and η = 14.33.

3.4 Cavity and void observations

The intensity of small angle X-ray scattering (SAXS) in deformed semicrystalline polymers such as iPP is known to be a superposition of contributions from scattering on periodic structures (crystalline-amorphous) and much more intense scattering from voids [14]. For specimens stretched beyond the yield point, the scattering profile ascribed to the periodic structure is concealed behind the scattering signals from voids [15].

Figure 7 shows SAXS 2D patterns for the drawn specimens stretched beyond the yield point in the stress-time curve at speeds of 45 and 170 mm/min. All the drawn directions are horizontal. According to these data, for all specimens the signals ascribed to a large fraction of voids suddenly appeared at smaller angles, consisting of two intense round lobes centered on the median in a peanut shell shape. This pattern corresponds to the signature from larger heterogeneities elongated with the long axis oriented perpendicular to the applied load [16]. Moreover, the intensity of scattering tends to increase at lower tensile speeds, indicating that the void size and volume show a positive dependence on the tensile speed. Figure 8 shows SAXS patterns for fracture specimens taken from the zone in the vicinity of the fracture cross-section drawn up to 170% of nominal strain. A rhombus or elliptical scattering pattern is seen in the vertical direction for the fracture specimens drawn at 45 or 170 mm/min tensile speed, respectively. According to figures 7 and 8, we find that as elongation proceeds, the orientation of the voids changed from perpendicular to parallel to the stretching direction. Further deformation led

the cavities to align along the deformation direction (maximum scattering is in the direction perpendicular to deformation). These patterns show that the cavities have been reoriented at a local strain of around 170%. [17].

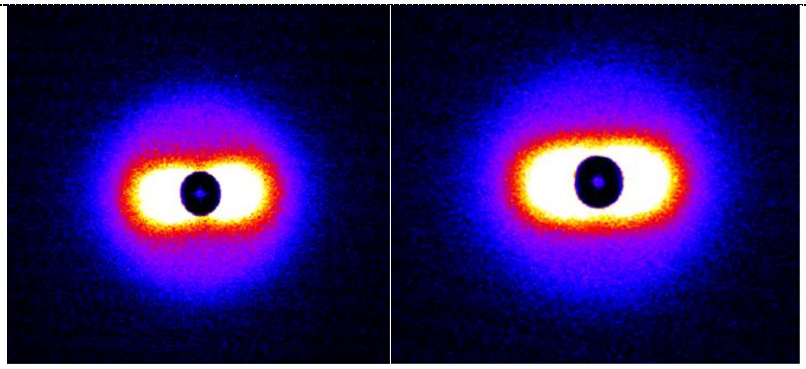

45 mm/min 170 mm/min

Figure 7. SAXS 2D patterns for drawn specimens stretched beyond the yield point in the stress-time curve, at speeds of 45 and 170 mm/min. The drawn direction is horizontal.

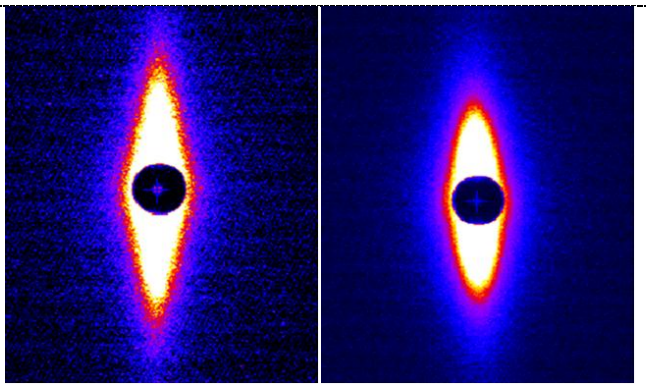

45 mm/min 170 mm/min

Figure 8. SAXS patterns for fracture specimens taken from the zone in the vicinity of the cross section. The drawn direction is horizontal.

To characterize the difference in features between the ductile and semi-brittle fractures, we performed scanning electron microscopic (SEM) imaging of the surface zone of specimens failed at speeds of 170 and 45 mm/min. To distinguish the different influences of intense and low tensile speeds, figure 9 shows SEM images of the surface zone of specimens failed at speeds of 170 and 45 mm/min. Similar void clusters separated by damaged and undamaged walls are detected perpendicular to the tensile direction on the surfaces for both kinds of specimens. There are more numerous and broader voids over the surface for the specimen stretched at 170 mm/min, compared with the one stretched at 45 mm/min. The same results can be visualized by polarized optical microscopy (figure 10). This means that, for specimens stretched at various tensile speeds, the fracture behavior is dominated by the propagation of voids and cavities. For similar void types, the opening and propagation speeds of the voids and cavities is proportional to the tensile speed, and thus the mean fracture time is inversely proportional to the tensile speed. When the specimen is stretched at extremely high tensile speed, voids and cavities coalescence as large voids appear and then propagate instantly, reducing the specimen lifetime. Thus, the probability of fracture increases, and the fracture time probability density distribution leans to the left.

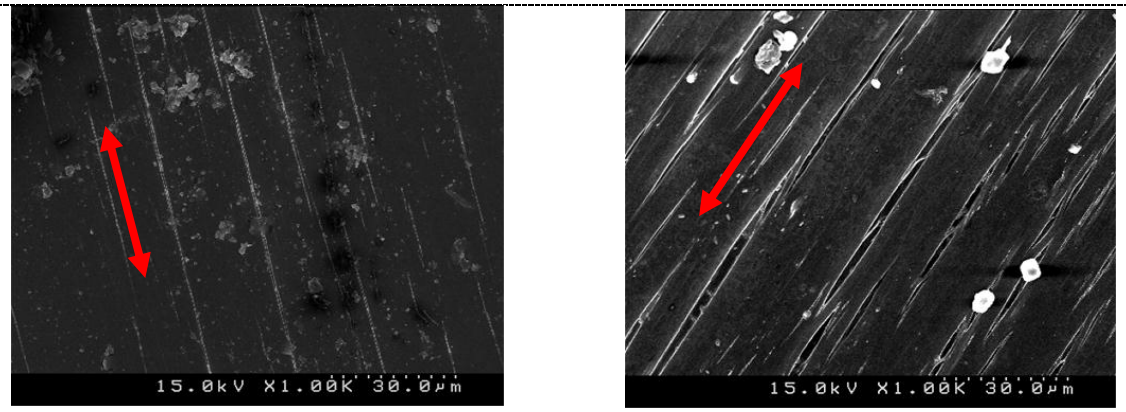

45 mm/min 170 mm/min

Figure 9. SEM images of the surface zone of specimens failed at speeds of 45 and 170 mm/min. The red arrows indicate the stretching direction.

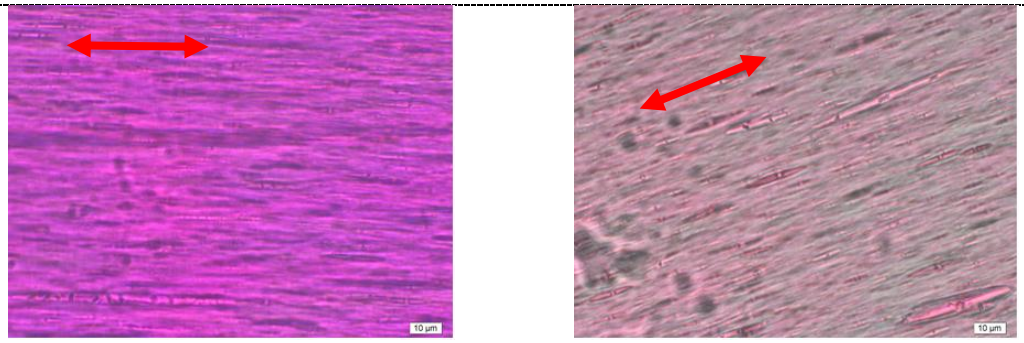

45 mm/min 170 mm/min

Figure 10. Polarized optical microscopic images of the surface zone of specimens failed at speeds of 45 and 170 mm/min. The red arrows indicate the stretching direction.

5. Conclusions

In this work, the statistical nature of tensile fracture for iPP materials under different tensile speeds was sd. Data collected from more than one hundred tensile tests were analyzed using Gaussian and Weibull distribution curves to quantify the nature of the data scattering. We have drawn the following conclusions:

1: The probability distribution curves of fracture time, strength, strain and toughness can be fit by Gaussian distribution functions.

2: The fracture time is inversely proportional to the tensile speed. The fracture time monotonously increases with increasing gauge length of the specimen.

3: The average fracture strength is more sensitive to gauge length than to tensile speed. Longer gauge length leads to larger average strength.

4: Toughness is an intrinsic characteristic, independent of tensile speed and gauge length, and is a possible criterion for fracture.

5: At crosshead speeds above 170 mm/min, the probability distribution function of the fracture time changed from a Gaussian to a Weibull distribution.

These fracture time distributions make it possible to predict precise safety factors based on the probability of fracture events. Consequently, we can define the service limitations of the material. This will provide important information for materials design, to improve the reliability and lifetime of the materials under various conditions.

References

[1] Nitta KH and Ishiboro T 2002 *J. Polym.Sci. Polym. Phy*.**40** 2018
[2] Gorus A 2012 *Analysis of reliability and quality control: fracture mechanics 1*(New York: Wiley)
[3] Bazant ZP 2004 *Proc. National Acad. Sci. USA* **101** 13400
[4] Phoenix SL 1978 *Int. J. Fracture* **14** 327
[5] Bazant ZP and Pang SD 2004 *Fracture Mechanics Concrete Structures* 189
[6] Freudenthal AM and Gumbel EJ 1959 J. Amer. Statist. Assol. **49** 575
[7] Weibull W 1951 *J. Appl. Mech.* 293
[8] Ben PY and Xu J 2011 *Polym. Eng. Sci.* **51** 574
[9] Kalman RE 1960 *Trans ASME J Basic Eng.* 35
[10] Rousu DN 1973 *Technometrics* **15** 927
[11] Kolmogoroff A 1931 *Math Annal* **104** 415
[12] Haward RN 1993 *Macromolecules* **26** 5860-5869.
[13] Zhang XC, Butler MF, Cameron RE 2000 *Polym* **41** 3797
[14] Allan P, Bevis M 1977 *Philos Mag* **35** 405
[15] Butler MF, Donald AM , Ryan AJ 1998 *Polymer* **39** 39
[16] Zhang XL, Botler MF and Cameron RE 2000 *Polym.* **41** 3797
[17] Pawlak A 2007 *Polym.* **48** 1397